Electronic and structural properties of two semi-Heusler alloys: NbIrSn and NbIrSb

1999 J. Phys.: Condens. Matter 11 6169

(http://iopscience.iop.org/0953-8984/11/32/308)

J. Phys.: Condens. Matter **11** (1999) 6169–6178. Printed in the UK PII: S0953-8984(99)03385-8

Electronic and structural properties of two semi-Heusler alloys: NbIrSn and NbIrSb

Michael Springborg†, Bernhard Sang‡ and Mari-Louise Persson‡

† Department of Chemistry, University of Konstanz, D-78457 Konstanz, Germany
‡ Department of Physics, University of Konstanz, D-78457 Konstanz, Germany

Received 13 April 1999, in final form 21 May 1999

Abstract. Using the LMTO-ASA (linearized muffin-tin orbital plus atomic-sphere approximation) method, we have calculated the structural and electronic properties of NbIrSn and NbIrSb. In contrast to the experimental finding, we find that NbIrSn has a band gap in excess of 1 eV. On the other hand, NbIrSb is a non-magnetic metal. The calculated lattice constants are in very good agreement with the experimental values. Removing the Ir atoms leads to larger contractions of the lattice constants and both materials become non-magnetic metals, whereas adding one extra Ir atom per formula unit leads to some expansion and, once again, the materials become non-magnetic metals. Finally, using the FLAPW (full-potential linearized-augmented-plane-wave) method as implemented in the WIEN programs we found that the results were essentially unaffected upon inclusion of the full potential or of spin–orbit couplings.

1. Introduction

A number of ternary compounds of the stoichiometry AB_2C crystallize in the Heusler-alloy structure, whereas others with the stoichiometry ABC crystallize in the semi-Heusler-alloy structure. Both structures can be considered as consisting of four interpenetrating fcc lattices (cf. figure 1) with, e.g., the origin of the A lattice at $(0, 0, 0)$, that of the C lattice at $(a/2, 0, 0)$, and, for the semi-Heusler alloys, the B lattice has its origin at $(a/4, a/4, a/4)$, whereas the lattice at $(a/4, a/4, 3a/4)$ is empty. For the Heusler alloys the vacancy sites are also occupied by B atoms.

Many of the Heusler and semi-Heusler alloys contain 3d transition-metal atoms and they are often either semiconductors with relatively large band gaps or (in some cases, magnetic) metals (see, e.g., [1–13]). Furthermore, some of the semi-Heusler alloys possess the unusual property that the electrons closest to the Fermi level are completely spin polarized with the result that the material is semiconducting for one spin component and metallic for the other [1].

Very recently Hohl *et al* [14] reported the synthesis of two new members of the semi-Heusler-alloy class, i.e. NbIrSn and NbIrSb. Compared with most other semi-Heusler alloys, these compounds contain no 3d transition-metal atoms and, moreover, for NbIrSn the authors reported an unusually small band gap, i.e., 0.28 eV, obtained by analysing the temperature dependence of the Seebeck coefficient. For NbIrSb the analysis was less unambiguous.

In this communication we shall extend the experimental analysis by reporting results of first-principles, density-functional calculations on the two semi-Heusler alloys NbIrSn and NbIrSb. We shall only consider the ordered structures of figure 1. Experimentally, the structure was determined from powder-diffraction measurements, but in such experiments it is very difficult to distinguish between ordered and random alloys. The possibility can therefore not

0953-8984/99/326169+10$30.00

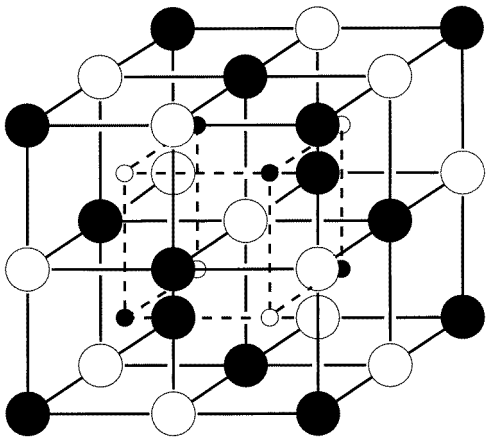

Figure 1. The structure of the Heusler and semi-Heusler alloys. The large white and black spheres represent A and C atoms. All small spheres represent B atoms for the Heusler alloys, whereas only half of them (all black or all white spheres) represent B atoms for the semi-Heusler alloys.

be excluded that the experimental samples contain some disorder. For instance, some of the vacancy sites may be occupied by B atoms (here Ir) or, alternatively, some of the B sites may be vacant. In order to get a first insight into the effects of such structural modifications we have here also considered the hypothetical structures NbSn and NbSb as well as $NbIr_2Sn$ and $NbIr_2Sb$ obtained by either removing all Ir atoms or by occupying all vacancy sites with Ir atoms. In the latter case we obtain an ordered Heusler alloy.

We shall concentrate on three issues: the optimized lattice constant as a function of composition, the electronic density of states, in particular closest to the Fermi level, as a function of composition, and the possible existence of a spin polarization. To this end we have applied two density-functional methods that will be briefly described in section 2. Section 3 contains the results and a conclusion is offered in section 4.

2. Computational methods

For each of the (six) compounds we first optimized the lattice constant using the LMTO-ASA (linearized muffin-tin orbital plus atomic-sphere approximation) method [15–17] without allowing for any spin polarization. Subsequently, for the optimized structure, we allowed the electrons to polarize, still using the LMTO-ASA method. Finally, for the two semi-Heusler alloys, we used the FLAPW (full-potential linearized-augmented-plane-wave) method as implemented in the WIEN programs [18] in checking whether the ASA of the LMTO-ASA method leads to unacceptable approximations in the density of states of the optimized structures as well as in studying the role of spin–orbit couplings, and to check whether this more accurate method produces other results concerning a possible spin polarization.

Both methods are based on the density-functional formalism of Hohenberg and Kohn [19] in the formulation of Kohn and Sham [20]. Then, the problem of calculating the total electronic energy is recast into that of solving the single-particle equations

$$\left[-\frac{\hbar^2}{2m}\nabla^2 + V(\vec{r}) \right] \psi_i(\vec{r}) = \epsilon_i \psi_i(\vec{r}). \tag{1}$$

Here, the potential

$$V(\vec{r}) = V_{\rm n}(\vec{r}) + V_{\rm C}(\vec{r}) + V_{\rm xc}(\vec{r}) + V_{\rm sr}(\vec{r}) \tag{2}$$

contains one term from the Coulomb potential of the nuclei, one from that of the electrons, the exchange–correlation potential (for which we in the present work use the local-density approximation of von Barth and Hedin [21]), and the scalar-relativistic potential (i.e., all relativistic effects up to second order in $1/c$ excluding the spin–orbit couplings).

For closely packed systems like those of the present study, the potential is approximately spherically symmetric about each site. Keeping only that part, one may solve equation (1) numerically inside (muffin-tin) spheres circumscribing each site for fixed energies ϵ_ν. For a given atom and (l, m), ϵ_ν is chosen as the centre of gravity of the atom- and angle-decomposed density of states. These functions together with their derivatives with respect to ϵ_ν form a set of (numerically given) basis functions that by construction are good approximations to the exact solutions to equation (1). Outside the spheres they are augmented continuously and differentiably with either spherical or plane waves.

Within the LMTO-ASA method the spheres are expanded so that their total volume equals that of the crystal and spherical waves are used in the interstitial region. Furthermore, only the spherically symmetric part of the potential is kept throughout the calculations. Finally, the effects of the overlaps of the spheres and of the interstitial region are included only perturbatively, whereby a highly efficient method results. For the systems of the present study we introduced so-called empty spheres at all sites of figure 1 that were not occupied by real atoms in order to reduce the effects of the sphere overlaps and of the interstitial region.

On the other hand, the WIEN programs are based on the FLAPW method and include the full potential in the calculations. They do not allow the spheres to overlap and employ plane waves in the interstitial region. Thereby, the method becomes computationally somewhat more demanding than the LMTO-ASA method, but also more accurate.

In the LMTO calculations we used 91 $\vec{k}$-points in the irreducible part of the Brillouin zone, whereas we used 30 $\vec{k}$-points in the WIEN calculations. Furthermore, in the LMTO calculations all (occupied and empty) spheres had the same radii except for the calculations on the NbSn and NbSb systems for which the radii of the empty spheres were 20.5% smaller than those of the other spheres. For the WIEN calculations the radii of the (non-overlapping) spheres were kept at $s_{\rm mt} = 2.5$ au. In the LMTO calculations, basis functions up to $l_{\rm max} = 3$ were included, but the Yb core of Ir and the Kr core of Nb, Sn, and Sb were kept frozen. In the WIEN calculations, all orbitals were allowed to relax, and in the interstitial region plane waves up to $s_{\rm mt}k_{\rm max} = 8$ were included. Finally, inside the spheres we used basis functions up to $l_{\rm max} = 10$.

3. Results

In table 1 we list the optimized lattice constants as obtained with the LMTO method together with the two experimental values for the semi-Heusler alloys. We observe a very good agreement between the experimental and theoretical values with, however, the difference that the calculations predict that the lattice constant for all Sn-based compounds is smaller than that of the equivalent Sb-based compounds in contrast to the experimental finding. Since the covalent radius of Sn is larger than that of Sb [22, 23] one would intuitively expect that the lattice constant of NbIrSn is larger than that of NbIrSb, in agreement with the experimental observations and in contrast to the theoretical ones, although the differences are indeed small. Finally, table 1 shows that for NbIrSn we find a small overestimate in the bond lengths, which is atypical for local-density calculations.

Table 1. Optimized (a_{opt}) and experimental (a_{exp}) values for the lattice constant together with the number of electrons inside the various muffin-tin spheres, q_X. q_X is the value for atom X (Sx being Sn and Sb and es being the empty spheres) and is calculated relative to the value for the neutral atom. The results were obtained with the LMTO method.

Compound	a_{opt} (au)	a_{exp} (au)	q_{Nb}	q_{Ir}	q_{Sx}	q_{es}
NbIrSn	11.59	11.68	−0.96	0.27	−0.69	1.38
$NbIr_2Sn$	12.06		−0.42	0.37	−0.31	
NbSn	10.36		−1.17		−0.75	0.96
NbIrSb	11.66	11.62	−0.86	0.32	−0.84	1.38
$NbIr_2Sb$	12.13		−0.42	0.44	−0.45	
NbSb	10.47		−1.08		−0.87	0.97

Adding one more Ir atom per formula unit (leading to AB_2C) gives only a smaller expansion of the unit cell. This may not be that surprising since the size of the vacancies for the ABC system is as large as that of the Ir atoms of that system and, therefore, the expansion is mainly determined by redistributions of the electrons. This can be quantified through the number of electrons inside the respective atomic spheres (cf. table 1). These show that about half of the electrons of the Nb and Sn/Sb atoms that were leaking out for the ABC systems are put back into those spheres for the AB_2C spheres.

On the other hand, when removing the Ir atoms (leading to AC) the lattice constant is considerably reduced. Although the Nb and Sb/Sn spheres in these calculations are larger, even fewer electrons are found inside those as for the ABC systems, as seen in table 1.

These changes in the electron density can also be observed in figure 2, where we show the electron density of the six compounds in the (1, 1, 0) plane. A careful inspection shows, e.g., how the electron density centred about the Nb atoms extends into the regions of the vacancies for the systems containing such vacancies.

The density of states (figure 3) shows that only one compound, NbIrSn, is semiconducting, whereas all others are metallic according to the LMTO calculations. When repeating the calculations for the optimized lattice constant but giving the systems small initial spin polarizations, all calculations converged to the unpolarized results of figure 3, which implies that the systems are non-magnetic.

The band gap of NbIrSn is calculated to be about 1 eV, but since density-functional calculations tend to underestimate this quantity, a realistic value is roughly 1.5 eV (a similar correction applied for crystalline silicon for which density-functional calculations predict a band gap of 0.52 eV compared with the experimental value of 1.17 eV [24]). This value is considerably larger than the experimental one of 0.28 eV [14], but is comparable with the values for other semiconducting semi-Heusler and Heusler alloys. When the material contains a small fraction of impurities and assuming that a rigid-band model is valid, the Fermi level will be shifted such that it appears in a region of a finite density of states. On the other hand, if some of the vacancies are occupied by Ir atoms and some of the Ir sites become vacant, the density of states will, to a first approximation, be a superposition of that of figure 3(a) plus small coefficients times those of figures 3(b) and 3(c) and, once again, there will be a finite density of states at the Fermi level.

When the number of impurities is small, they will induce states in the gap of figure 3(a). But since these states are localized to the regions of the impurities they will rather act as traps for transport properties and can therefore not explain the temperature dependence of

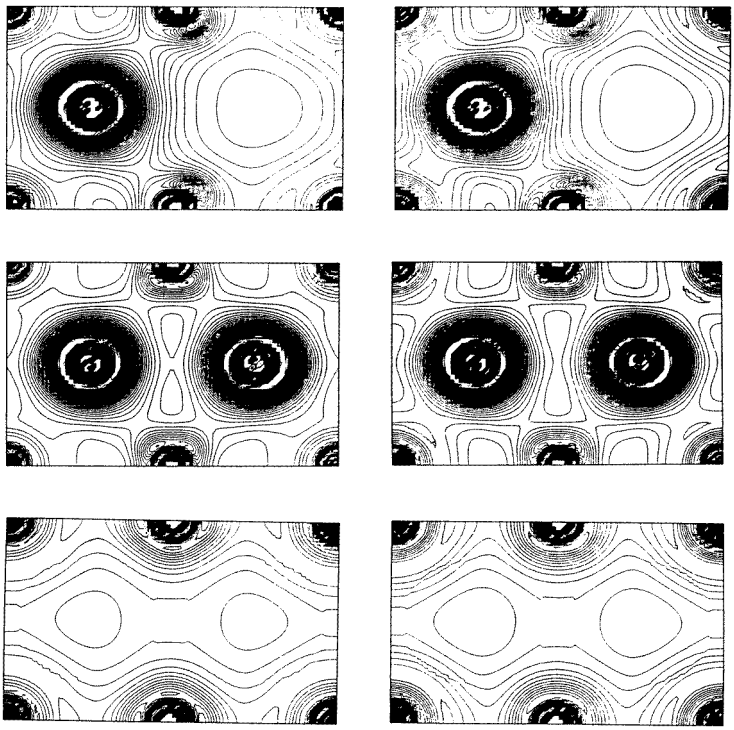

Figure 2. The total electron density for (left column) the Sn-based and (right column) the Sb-based compounds for (top) ABC, (middle) AB_2C, and (bottom) AC. The figures are shown in the (1, 1, 0) plane of figure 1, and include 41 equally spaced values between 0.0 and 0.3 au. Sn and Sb atoms are placed at the corners and Nb atoms at the centres of the horizontal axes. The results have been obtained with the LMTO method.

the Seebeck coefficient which suggests the existence of a small band gap. Thus, we have to conclude that the results of figure 3 for the Sn-based systems are not able to explain the experimental band gap.

For the Sb-based systems we find that they are all metallic. Moreover, the Fermi level appears in all cases at a position of a relatively high density of states, and, for NbIrSb, only for a large doping concentration can it be shifted to either a gap (p doping) or to a lower density of states (n doping).

In figure 4 we show the decomposed densities of states for the two ABC compounds. They show that the lowest valence bands (below roughly -6 to -10 eV) are mainly due to Sn or Sb functions, and that the lowest conduction bands (just above the energy zero) are due to Nb functions. The absolutely highest valence bands have large components on Nb, too, but also some contributions from Sn or Sb and Ir, whereas Ir functions are responsible for a major part of the sharp features in the broad energy range of occupied orbitals from about -6 eV to the Fermi level. Finally, the empty spheres contribute only insignificantly to the total density of states.

As a first approximation, the overall features of figure 4 prevail also for the other compounds, which makes an interpretation of the results of figure 3 obvious. There are, however, modifications. For example, the size of the gap between the lowest valence band and the next higher one (i.e., in the energy range -6 to -10 eV), as well as the position of the

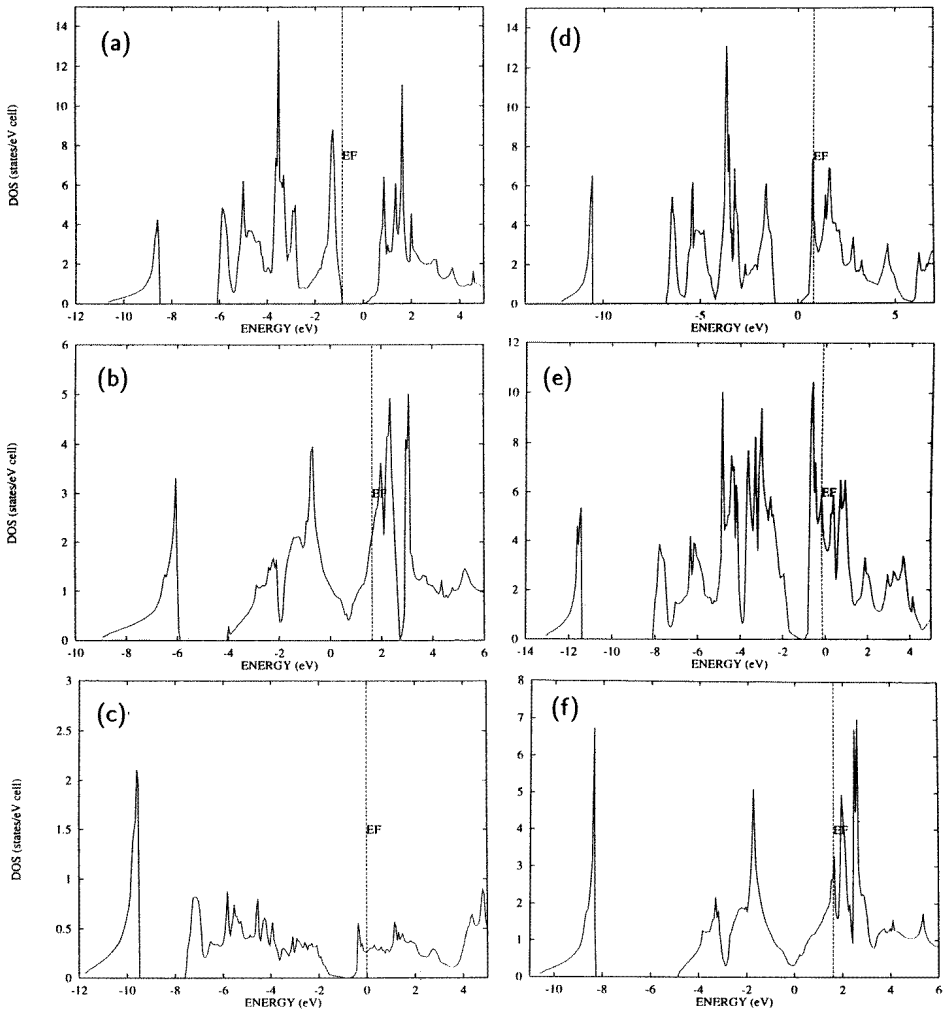

Figure 3. The valence-electron density of states for the optimized structures of (a) NbIrSn, (b) $NbIr_2Sn$, (c) NbSn, (d) NbIrSb, (e) $NbIr_2Sb$, and (f) NbSb. The vertical dashed lines mark the Fermi level. The results have been obtained with the LMTO method. Please notice that the ordinate scales of the different panels differ.

lowest valence band relative to the Fermi level, depends on the stoichiometry.

The band structures of the two semi-Heusler alloys are shown in figure 5. They are very similar and, to a first approximation, the changes when passing from Sn to Sb can be treated within a rigid-band approximation. NbIrSn is seen to be an indirect-gap semiconductor, and in particular the highest occupied band is very flat.

The LMTO calculations have led to results for the semi-Heusler alloys that are very similar to those for other semi-Heusler alloys, although there are some discrepancies compared with the experimental findings, in particular concerning the size of the gap of NbIrSn. Mohn *et al* [8] found that in some cases the ASA could lead to wrong results (e.g., for magnetic properties) for such compounds. Therefore, we also carried out full-potential calculations using the WIEN programs, but only for those lattice constants that were optimized with the LMTO programs

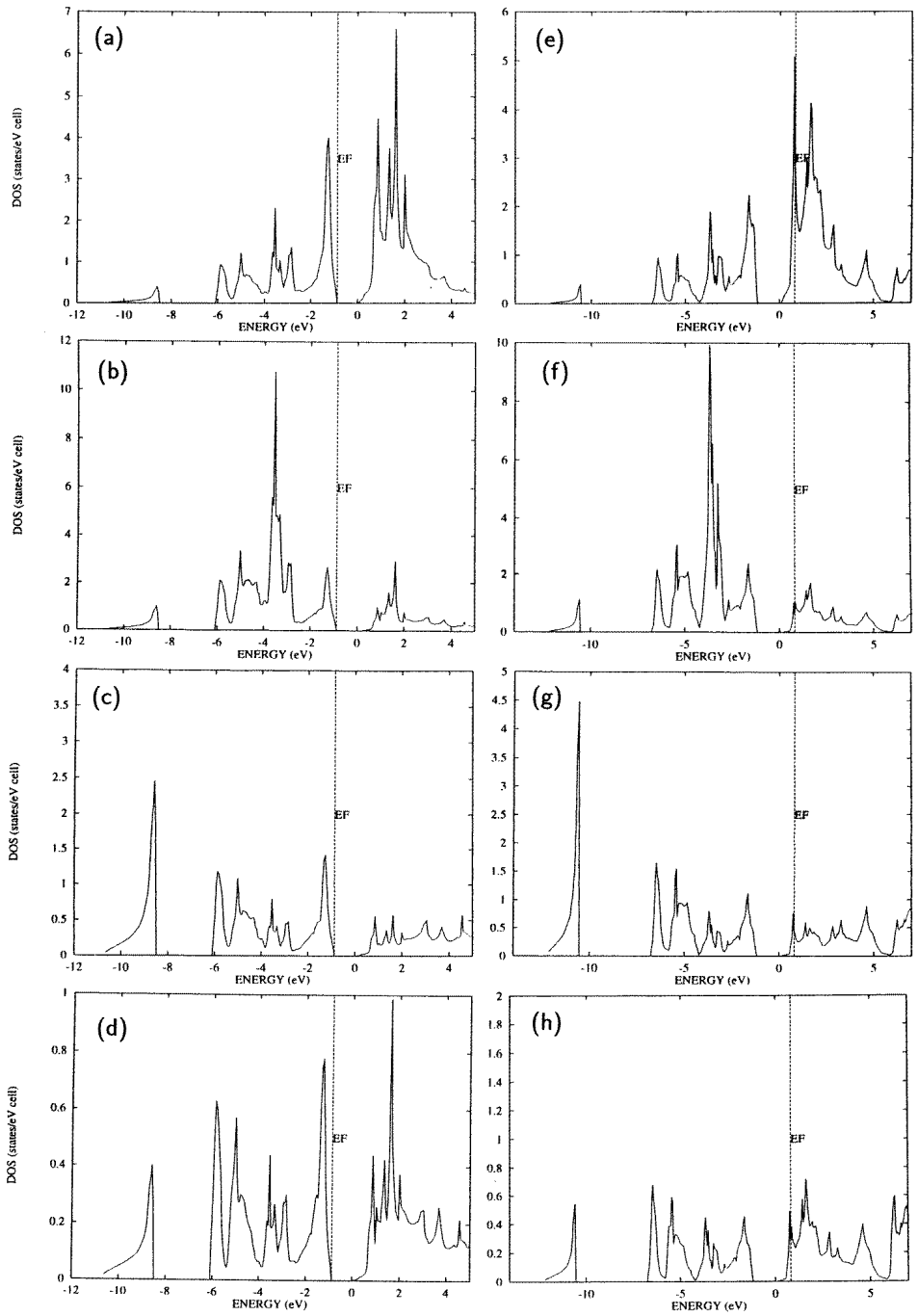

Figure 4. The valence-electron density of states for the optimized structures of ((a)–(d)) NbIrSn and ((e)–(h)) NbIrSb decomposed into the contributions from ((a), (e)) Nb, ((b), (f)) Ir, (c) Sn, (g) Sb, and ((d), (h)) the empty spheres. The vertical dashed lines mark the Fermi level. The results have been obtained with the LMTO method. Please notice that the ordinate scales of the different panels differ.

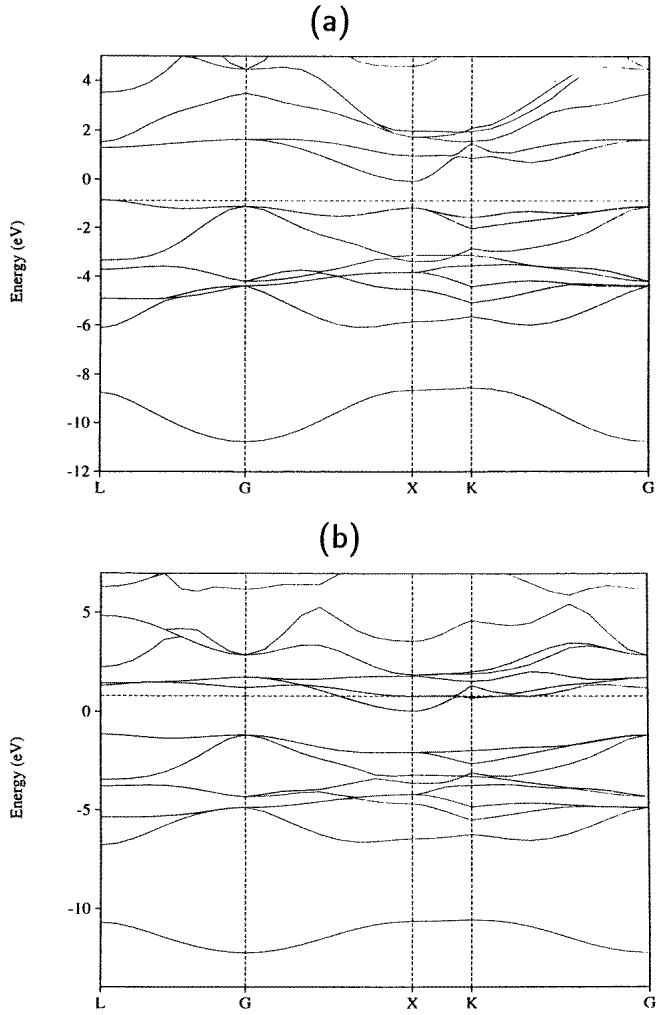

Figure 5. The band structures for the optimized structures of (a) NbIrSn and (b) NbIrSb along some high-symmetry lines. The results have been obtained with the LMTO method, and G = Γ.

for the two semi-Heusler alloys. Figures 6(a) and 6(c) show the resulting density of states and compared with the similar results from the LMTO calculations (figures 2(a) and 2(d)) the differences are only insignificant and mainly due to differences in $\vec{k}$-space sampling and in the energy mesh. Subsequently, we allowed for a spin polarization, but in this case also the calculations converged to a non-magnetic structure.

Finally, we checked whether the inclusion of spin–orbit couplings would change the results but, as seen in figures 6(b) and 6(d), this is not the case. Ir is the heaviest of the elements involved and, therefore, the largest changes in the density of states occur where the Ir-centred functions have their largest contributions, which is in the centre of the upper occupied valence bands; cf. figure 3. In total, the spin–orbit couplings tend to lead to some smearing out of the features of the density of states without leading to any overall broadening or changes in the gaps.

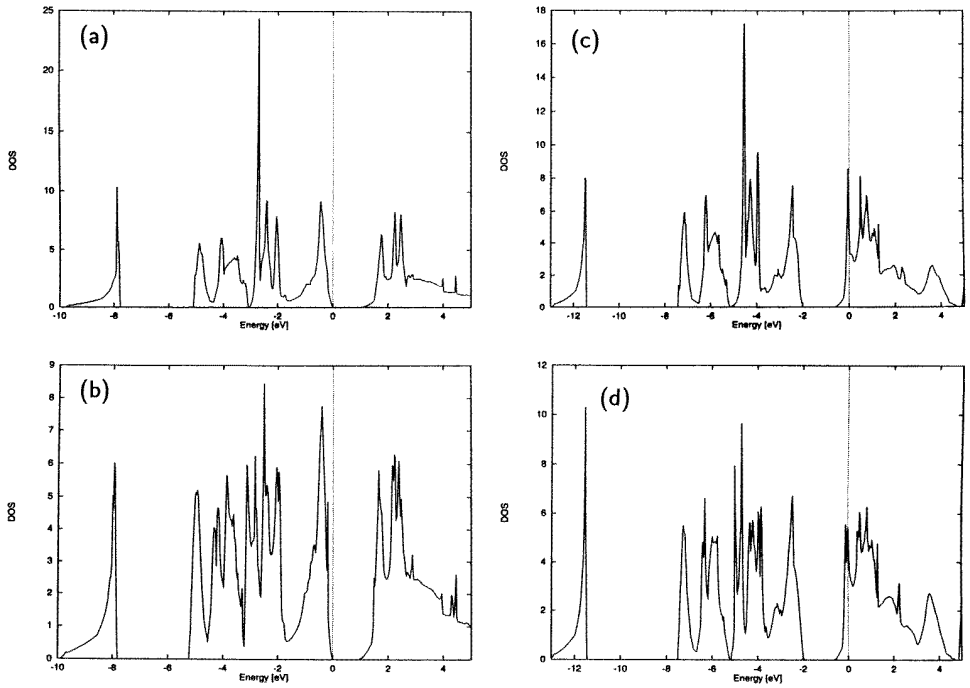

Figure 6. Densities of states for ((a), (b)) NbIrSn and ((c), (d)) NbIrSb ((a), (c)) without and ((b), (d)) with inclusion of spin–orbit couplings. The results have been obtained with the WIEN programs and the vertical dashed lines mark the Fermi levels which have been placed at the energy zero. Please notice that the ordinate scales of the different panels differ.

4. Conclusions

Using two density-functional methods we have calculated electronic and structural properties of the two title compounds in their ordered phases. We found that NbIrSn is a semiconductor with a gap that should be in excess of 1 eV, whereas NbIrSb is a non-magnetic metal. An accurate treatment of all effects of the potential and of spin–orbit couplings does not change these conclusions. The experimentally produced materials may be less ordered. This could, e.g., lead to local arrangements of the type NbSn and $NbIr_2Sn$ (or NbSb and $NbIr_2Sb$) and we, therefore, considered also the ordered structures of those systems. These were found in all cases to be non-magnetic metals with lattice constants that are somewhat smaller for NbSn and NbSb and slightly larger for $NbIr_2Sn$ and $NbIr_2Sb$ when compared with NbIrSn and NbIrSb. However, the results for these systems do not support the suggestion that the experimentally found small value of the band gap of NbIrSn is due to some disorder or impurities. Finally, the bands are fairly flat suggesting that these materials possess poor transport properties. Disorder will worsen these even further.

Acknowledgment

One of the authors (MS) is grateful to Fonds der Chemischen Industrie for its very generous support.

References

[1] de Groot R A, Mueller F M, van Engen P G and Buschow K H J 1983 *Phys. Rev. Lett.* **50** 2024
[2] Kübler J, Williams A R and Sommers C B 1983 *Phys. Rev.* B **28** 1745
[3] Ishida S, Asano S and Ishida J 1984 *J. Phys. Soc. Japan* **53** 2718
[4] da Silva E Z, Jepsen O and Andersen O K 1988 *Solid State Commun.* **67** 13
[5] Wijngaard J H, Haas C and de Groot R A 1989 *Phys. Rev.* B **40** 9318
[6] Lin W and Freeman A J 1992 *Phys. Rev.* B **45** 61
[7] Morán-López J L, Rodríguez-Alba R and Aguilera-Granja F 1994 *J. Magn. Magn. Mater.* **131** 417
[8] Mohn P, Blaha P and Schwarz K 1995 *J. Magn. Magn. Mater.* **140–144** 183
[9] Tobola J, Pierre J, Kaprzyk S, Skolozdra R V and Kouacou M A 1996 *J. Magn. Magn. Mater.* **159** 192
[10] Kaczmarska K, Pierre J, Beille J, Tobola J, Skolozdra R V and Melnik G A 1998 *J. Magn. Magn. Mater.* **187** 210
[11] Tobola J, Pierre J, Kaprzyk S, Skolozdra R V and Kouacou M A 1998 *J. Phys.: Condens. Matter* **10** 1013
[12] Ślebarski A, Jezierski A, Lütkehoff S and Neumann M 1998 *Phys. Rev.* B **57** 6408
[13] Singh D J and Mazin I I 1998 *Phys. Rev.* B **57** 14 352
[14] Hohl H, Ramirez A P, Goldmann C, Ernst G, Wölfing B and Bucher E 1998 *J. Phys.: Condens. Matter* **10** 7843
[15] Andersen O K 1975 *Phys. Rev.* B **12** 3060
[16] Andersen O K and Jepsen O 1984 *Phys. Rev. Lett.* **53** 2571
[17] Skriver H L 1984 *The LMTO Method* (Berlin: Springer)
[18] Blaha P, Schwarz K and Luitz J 1997 *WIEN97* Vienna University of Technology
This is an improved and updated Unix version of the original copyrighted WIEN code, which was published by Blaha P, Schwarz K, Sorantin P and Trickey S B 1990 *Comput. Phys. Commun.* **59** 399
[19] Hohenberg P and Kohn W 1964 *Phys. Rev.* **136** B864
[20] Kohn W and Sham L J 1965 *Phys. Rev.* **140** A1133
[21] von Barth U and Hedin L 1972 *J. Phys. C: Solid State Phys.* **5** 1629
[22] Pauling L 1960 *The Nature of the Chemical Bond* (Ithaca, NY: Cornell University Press)
[23] Harrison W A 1980 *Electronic Structure and the Properties of Solids* (San Francisco, CA: Freeman)
[24] Hybertsen M S and Louie S G 1986 *Phys. Rev.* B **34** 5390